Eur. Phys. J. D **44**, 515–524 (2007)
DOI: 10.1140/epjd/e2007-00186-5

THE EUROPEAN PHYSICAL JOURNAL D

Structural properties of amorphous TiO_2 nanoparticles

V.V. Hoang[1,a], H. Zung[2], and N.H.B. Trong[3]

[1] Dept. of Physics, Institute of Technology, National Univ. of HochiMinh City, 268 Ly Thuong Kiet Str., Distr. 10, HochiMinh City, Vietnam
[2] Dept. of Science and Technology, National Univ. of HochiMinh City, HochiMinh City, Vietnam
[3] Dept. of Mater. Sci., College of Natural Sci., Natl. Univ. of HochiMinh City, HochiMinh City, Vietnam

Received 16 November 2006 / Received in final form 30 March 2007
Published online 8 June 2007 –

Abstract. Structural properties of amorphous TiO_2 spherical nanoparticles have been studied in models with different sizes of 2 nm, 3 nm, 4 nm and 5 nm under non-periodic boundary conditions. We use the pairwise interatomic potentials proposed by Matsui and Akaogi. Models have been obtained by cooling from the melt via molecular dynamics (MD) simulation. Structural properties of an amorphous nanoparticle obtained at 350 K have been analyzed in detail through the partial radial distribution functions (PRDFs), coordination number distributions, bond-angle distributions and interatomic distances. Moreover, we show the radial density profile in a nanoparticle. Calculations show that size effects on structure of a model are significant and that if the size is larger than 3 nm, amorphous TiO_2 nanoparticles have a distorted octahedral network structure with the mean coordination number $Z_{\mathrm{Ti-O}} \approx 6.0$ and $Z_{\mathrm{O-Ti}} \approx 3.0$ like those observed in the bulk. Surface structure and surface energy of nanoparticles have been obtained and presented.

PACS. 61.46.-w Nanoscale materials – 61.20.Ja Computer simulation of liquid structure – 78.55.Qr Amorphous materials; glasses and other disordered solids – 61.43.Bn Structural modeling: serial-addition models, computer simulation

1 Introduction

TiO_2 nanoparticles are of great interest for a variety of technological applications such as photocatalysis, photochemical solar cells, optoelectronic devices, chemical sensors, dielectric material of ultrathin-film capacitors and bioprobes [1–10]. Moreover, TiO_2 nanoparticles have been also used as raw material in electronic and structural ceramics [11], or as a removal of toxic contaminants from wastewater [10,12]. Nanocrystalline TiO_2 exists in several polymorphic forms, including amorphous, anatase and rutile depending on fabricating conditions and further heat treatment [13,14]. Due to the enormous technological importance, TiO_2 nanoparticles have been under intensive investigation for the past years by both experiments and computer simulations (see Refs. [1–49] and references therein). Nanosized-TiO_2 is mainly manufactured by either dry or wet processes [17,19,25,26,36]. The dry process involves vapor phase oxidation reaction of $TiCl_4$, which leads to the production of amorphous nanosized-TiO_2. The obtained amorphous nanosized-TiO_2 is then annealed at different temperatures to get desired crystalline phases such as anatase or rutile. Reaction involved in this process can be represented as follows: $TiCl_4(g) + O_2(g) \rightarrow TiO_2(s) + 2Cl_2(g)$. Particularly, TiO_2 nanoparticles have been produced by the controlled hydrolysis of tetraisopropyltitanate in sodium bis (2-ethylhexyl) sulfosuccinate reverse micelles and these nanoparticles aggregated into sols with colloid sizes of 20 nm to 200 nm [16]. And different titania phases were produced depending on the size of the micellar water pool: small pools yielded amorphous particles, while larger pools produced anatase [16]. Sol-gel TiO_2 nanoparticles with different phases such as amorphous, anatase and rutile were investigated in more details by optical techniques, by systematically varying synthesis, sample handling, and annealing variables [17]. Much attention has been spent to annealing-induced phase transformation from amorphous nanosized-TiO_2 to nanocrystaline ones (i.e. anatase or rutile) [17–19,21,23,25,36–38,42,46,49]. It was found annealing-induced phase transformation from amorphous nanosized-TiO_2 to anatase and to rutile via Raman scattering, infrared reflectivity, infrared absorption, X-ray diffraction, and electron energy-loss spectroscopy [17]. Similar trends can be found in other work, particularly, a kinetic model for transformation from amorphous nanosized-TiO_2 to anatase has been proposed in order to highlight some aspects of such transformation, which has been often observed in practice by annealing the former [49]. On the other hand, electronic structure, electronic properties or ground states of nanosized-TiO_2 attract great interest [15,40,47]. The trap-limited

[a] e-mail: vvhoang2002@yahoo.com

electronic transport in assemblies of nanosized-TiO_2 particles were investigated by intensity modulated photocurrent spectroscopy and it was found that electronic transport is controlled by trapping and detrapping of photogenerated electrons in interfacial band-gap states, distributed in energy [15]. Barnard et al. presented the modeling structure and electronic properties of anatase TiO_2 nanoparticles by using a self-consistent tight-binding method and density functional theory and they found nonbonding electrons at the edges and corners of the nanoparticles [47]. Generally, structure and properties of nanoparticles greatly depend on their size. Indeed, size effects on Raman spectrum of nanocrystalline anatase TiO_2 or on pressure-induced amorphization in nanoscaled-TiO_2 have been found [34,45]. Moreover, it was found that the phase transition from amorphous to anatase nanosized-TiO_2 is also size dependent [17] and some structural, electronic and energetic trends as a function of nanoparticle size are also reported [47]. It is interesting to carry out the research in this direction in order to highlight the reason of the size dependence of various properties of nanoparticles. On the other hand, effects of amorphous content and particles size on the photocatalytic properties of TiO_2 nanoparticles have been observed in that for nanoparticles mainly in the anatase phases and mixed-phases, their photocatalytic activities increase significantly with decreasing amorphous content. This indicates that due to specific short-range order structure of amorphous phase, differed from those of crystalline ones, properties of TiO_2 nanoparticles can be changed by varying content of the former [20]. On the other hand, more details about the structure and properties including thermodynamics of nanoparticles can be obtained only via computer simulation and brief review can be done here. In order to simulate structure and properties of nanoparticles, one needs correct interatomic potentials. And, force field parameters for TiO_2-H_2O systems have been tested by ab initio calculations, particularly, force fields for TiO_2 surfaces in a vacuum have been found [27]. Further, thermodynamic model has been proposed for describing the shape of TiO_2 nanoparticles as a function of size in order to predict their phase stability [29]. By using density functional calculations the surface energies and surface tensions of TiO_2 nanoparticles were found, and it was found that surface passivation has an important impact on nanocrystal morphology and phase stability of TiO_2 nanoparticles [29]. As discussed above, structure and electronic properties of anatase TiO_2 nanoparticles have been calculated by Barnard et al. [47]. However, in order to understand different properties of nanoparticles, it needs the knowledge of their microscopic structure, which can be provided only by computer simulation and systematic analysis of microstructure of TiO_2 nanoparticles has not been done yet although several results regarding microstructure of crystalline TiO_2 nanoparticles can be found by using MD simulation models with Matsui-Akaogi interatomic potentials [35].

One can see that although amorphous TiO_2 nanoparticles have been obtained in practice and it is clearly that their properties strongly differ from those of the crystalline analogs due to specific short-range order structure (see Refs. [15–49] and reference therein), their microscopic structure and properties have not been investigated in details yet. Because the size, phase and morphology of the TiO_2 nanoparticles have been found to be critical parameters determining their suitability for particular applications [50–52], therefore, it is worth to study microstructure and various properties of amorphous TiO_2 nanoparticles by computer simulation. And our main aim here is a systematic analysis of microstructure of amorphous TiO_2 nanoparticles with different sizes. Surface energy of amorphous TiO_2nanoparticles has been found and discussed. In addition, while it was spent less attention to the amorphous nanomaterials compared with those for nanocrystalline ones [53–55], our results provide additional understanding of structure of such important class of materials.

2 Calculation

It is very important to choose appropriate interatomic potentials for the system to be simulated. There are no potentials for liquid and amorphous TiO_2, however, there were several ones for the bulk crystalline TiO_2 [56–65]. Via detailed analysis of the different force fields for TiO_2, Collins et al. concluded that the force field developed for crystalline TiO_2 proposed by Matsui and Akaogi is the most suitable for MD simulating of the bulk TiO_2 [56,66]. For convenience we call these potentials the MA ones. The MA potentials are composed of the pairwise additive Coulomb, dispersion and repulsion interactions. The energy parameters of MA potentials were determined to reproduce the crystal structures of rutile, anatase and brookite, and the measured elastic constants of rutile. By using such potentials they successfully reproduced a wide range of properties of the different polymorphs of TiO_2 crystals mentioned above including the crystal structures, volume compressibility, volume thermal expansivities and enthalpy relationships between them [56]. After intensive testing we found that MA potentials are good for simulating liquid and amorphous TiO_2 and it was found that calculated data agree well with the experimental ones, i.e. amorphous TiO_2 has a distorted octahedral network structure with the mean coordination number $Z_{\mathrm{Ti-O}} \approx 6.0$ and $Z_{\mathrm{O-Ti}} \approx 3.0$ like those observed by experiments [67]. Moreover, the suitability of MA potentials for surface studies has been tested by using quantum mechanical methods [27]. It is essential to notice that in order to improve the suitability of MA potentials for nanoparticles, additional parameters of Buckingham potential for surface atoms in TiO_2 nanoparticles have been proposed [i.e. only the value for parameter $A_{ij} = f(B_i + B_j)$ in MA potentials has been slightly modified for surface atoms, see below in Eq. (1)]. Due to different local environments of atoms at the surface of nanoparticles compared with those in the core or in the bulk, such approach is important. However, the approach used in [27] is simply and it needs further improvement in this direction, especially for amorphous surfaces whereas local environments of atoms are much complex than those of nanocrystalline systems. Therefore,

Table 1. Energy parameters of MA potentials.

	A (Å)	B (Å)	C (Å^3 kJ$^{\frac{1}{2}}$ mol$^{-\frac{1}{2}}$)
Ti	1.1823	0.077	22.5
O	1.6339	0.117	54.0

in most cases the slight modification of interatomic potentials for surface atoms in nanosized-systems has not been done. The modification of parameters of Buckingham potential for surface atoms in TiO_2 nanoparticles has not been used later in simulation of anatase TiO_2 nanoparticles [35]. Fixed interatomic potentials for all atoms in different nanosized systems was preferred and one can estimate the suitability of interatomic potentials for surface via comparison of calculated surface energy with the experimental one [68–71]. Moreover, TiO_2 is an ionocovalent system and it must be considered in simulation. Numerous experimental studies of oxide systems indicate a substantial contribution of ionic bonding to interaction due to high electronegativity of the oxygen atoms [72], while covalent bonding is also important. The covalent interaction is described in terms of three-particle potentials, which significantly increase the computation time. Since ionic contribution cannot be neglected for oxides, the Coulomb interactions have to be considered. Simulation of oxide systems with mixed ionic and covalent bonds requires too many force parameters that it is very difficult to carry out. Therefore, the models have to be simplified and the choice of model based on the ionic interactions has significant advantages. Simulation results for oxide systems by using ionic model for the past three decades including our recent simulation for liquid and amorphous TiO_2 by using MA potentials confirmed this point (see [67,72–78] and references therein). Therefore, one can infer that MA interatomic potentials describe well both the bulk and the surface of crystalline or amorphous TiO_2 and we use them again here for simulating amorphous TiO_2 nanoparticles without slight modification for surface atoms, the MA potentials have the following form:

$$U_{ij}(r) = Z_i Z_j \frac{e^2}{r} + f(B_i + B_j) \times \exp\left[\frac{A_i + A_j - r}{B_i + B_j}\right] - \frac{C_i C_j}{r^6} \quad (1)$$

with i, j = Ti, O. Here r is the interatomic distance and Z_i, Z_j are the charges of ions: $Z_{\mathrm{Ti}} = +2.196$ and $Z_{\mathrm{O}} = -1.098$. The quantity f is a standard force of 4.184 kJ Å^{-1} mol^{-1}. Other parameters of potentials are shown in Table 1. More details about the MA potentials can be found in [56].

Coulomb interactions were taken into account by means of Ewald-Hansen method [75]. The simulations were done in a spherical particle with four different sizes of 2 nm, 3 nm, 4 nm and 5 nm, which contains the number of atoms corresponding TiO_2 stoichiometry and at the real density of 3.80 g/cm^3 for amorphous TiO_2 [79]. We first placed randomly N atoms in a sphere of fixed radius and

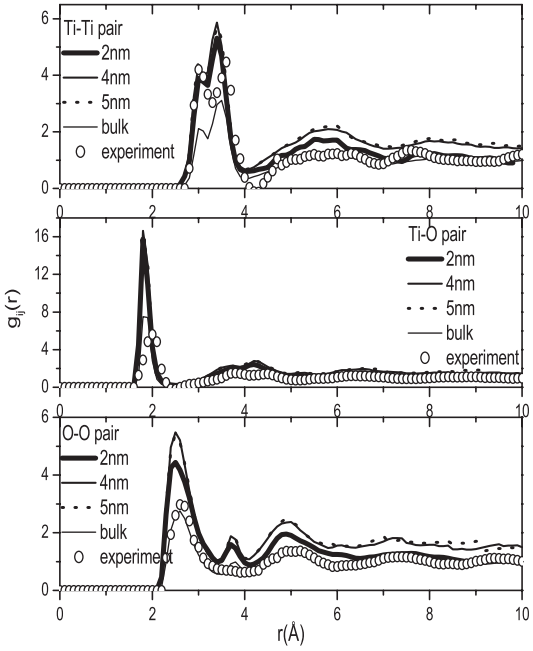

Fig. 1. Radial distribution functions of amorphous TiO_2 nanoparticles at 350 K, bulk and experiment for the bulk at $T = 350$ K (the calculated data for the amorphous bulk were taken from [67] and experimental data were taken from [80]).

the configuration has been relaxed for 50 000 MD steps at 7 000 K under non-periodic boundary conditions. The MD time step is of 1.6 fs and the system was cooling down from the melt at constant volume corresponding to the system density of 3.80 g/cm^3. Temperature of the system was decreased linearly in time as $T = T_0 - \gamma t$, here γ is a cooling rate of 4.2945×10^{13} K/s and T_0 is the initial temperature of 7 000 K. In order to calculate the coordination number and bond-angle distributions in amorphous TiO_2 nanoparticles, we adopt the fixed values $R_{\mathrm{Ti-T_i}} = 4.00$ Å, $R_{\mathrm{Ti-O}} = 2.50$ Å and $R_{\mathrm{O-O}} = 3.50$ Å. Here R denotes a cutoff radius, which is chosen as the position of the minimum after the first peak in PRDFs for the amorphous bulk at 350 K. The amorphous model at 350 K has been relaxed for 50 000 MD steps before evaluating static quantities. In order to improve the statistics of the simulation, the results have been averaged over two independent runs for nanoparticles with the size of 2 nm, 3 nm and 4 nm. Due to large number of atoms in the model with the size of 5 nm (i.e. 5626 atoms) single run was done for this size.

3 Results and discussions

3.1 Structural properties of amorphous TiO_2 nanoparticles compared with those observed in the bulk

The first quantity we would like to discuss here is the PRDF for different atomic pairs. As shown in Figure 1 and Table 2, the position of the first peaks in PRDFs

Table 2. Structural characteristics of amorphous TiO_2 at $T = 350$ K; r_{ij} — position of the first peaks in PRDFs; g_{ij} — the height of the first peaks in PRDFs; Z_{ij} — the average coordination number (numbers 1 and 2 denote Ti and O, respectively).

Materials	r_{ij} (Å)			g_{ij}			Z_{ij}			
	1-1	1-2	2-2	1-1	1-2	2-2	1-1	1-2	2-1	2-2
2 nm	3.00-3.40	1.82	2.49	5.31	16.08	4.44	7.31	5.30	2.65	8.97
3 nm	3.00-3.42	1.83	2.53	5.11	16.65	5.03	8.11	5.56	2.78	9.77
4 nm	3.00-3.39	1.83	2.52	5.87	17.31	5.49	8.61	5.71	2.85	10.33
5 nm	3.00-3.41	1.83	2.52	5.78	16.93	5.46	8.79	5.77	2.88	10.52
Bulk model [67]	3.00-3.47	1.85	2.59	3.15	8.27	2.75	8.92	5.76	2.88	10.70
Exp. for the bulk [80]	3.00-3.55	1.96	2.67	4.47	5.60	2.97	8.80	5.40	2.70	10.50

Table 3. Fraction of Ti atoms with corresponding coordination number $Z_{\mathrm{Ti-O}}$ in models obtained at $T = 350$ K.

Materials	$Z_{\mathrm{Ti-O}}$					
	3	4	5	6	7	8
2 nm	0.075	0.092	0.333	0.400	0.092	0.008
3 nm	0.010	0.094	0.291	0.543	0.062	0.000
4 nm	0.003	0.045	0.269	0.597	0.083	0.003
5 nm	0.006	0.026	0.242	0.650	0.074	0.002
The bulk [67]	0.000	0.006	0.279	0.668	0.045	0.002

changes slightly with particle size and it has smaller value compared with those for the bulk. In contrast, the height of peaks changes with size of nanoparticles however, the change is not systematic. The peaks in PRDF of nanoparticles is broader than that for the bulk indicating that structure of amorphous nanoparticles is more heterogeneous than that for the bulk due to the contribution of surface structure of the formers. One can see in Figure 1 that splitting of the first peak in PRDF for the Ti-Ti pair is also found in amorphous TiO_2 nanoparticles like those observed in experiment for the bulk [80]. The prepeak is centered at around 3.00 Å and the main peak is at 3.47 Å versus 3.00 Å and 3.55 Å obtained in experiment, respectively (see Tab. 2). As discussed in [80], the shorter Ti-Ti interatomic distance of 3.00 Å is related to the pairs of Ti atoms centering octahedra linking by the edge, the longer one of 3.55 Å is of pairs of Ti atoms from octahedra having a common vertex. This means that the linking of octahedra by the edge or vertex also exists in amorphous nanoparticles. As discussed in [67], the value 1.85 Å obtained for Ti-O bond length is in accordance to a distorted octahedral network structure in amorphous TiO_2 bulk model with significant amount of TiO_5. Concerning on the amorphous TiO_2 nanoparticles, due to the surface effects, i.e. leading to increase of number of undercoordinated structural units such as TiO_3, TiO_4 and TiO_5 in nanoparticles, the Ti-O bond length in nanoparticles is equal to around 1.82 Å, which is much lower than that for the bulk. And it is closer to those for tetrahedral coordinated Ti-O network [81,82]. One can see this tendency via the mean coordination number for different atomic pairs presented in Table 2, which increases with the size of nanoparticles. And for the size of 5 nm, the mean coordination number for all atomic pairs is close to that for the bulk (see Tabs. 2 and 3). In addition, occurrence of small peak at around 3.70 Å in PRDF for the O-O pair has

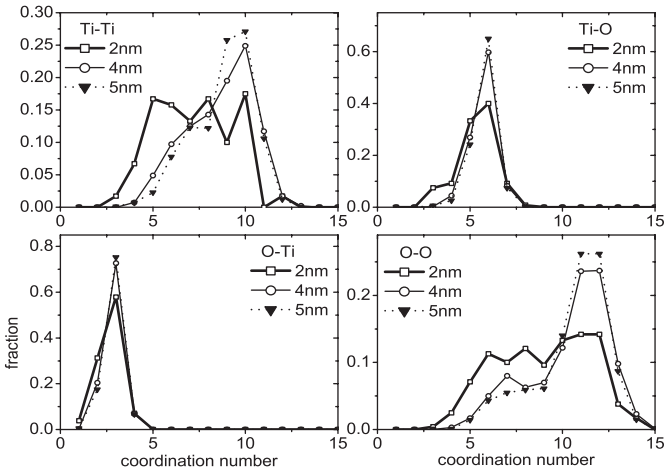

Fig. 2. Coordination number distributions of amorphous TiO_2 nanoparticles at $T = 350$ K.

been found in both the bulk and nanoparticles, which was also found experimentally in TiO_2 layers obtained by sol-gel dip coating [80]. For the amorphous bulk models such small peak occurs only in the low temperature-octahedral phases of the model together with the appearance of a prepeak at short distance in PRDF for the Ti-Ti pair [67]. Possibly, such small peak is related to the typical O-O distance of the octahedra linked by the edge in the system at low temperatures.

More details about the structure of nanoparticles can be found via the coordination number and bond-angle distributions (Figs. 2, 3). One can see that coordination number distributions strongly depend on the size of particles and if the size is larger than 4 nm the distributions are close with each other and with those for the bulk [67]. For the bond-angle, we present only the most important ones, i.e. Ti-O-Ti and O-Ti-O angles. The first one describes the connectivity between structural units TiO_n in the system and the second one describes the order inside them. Figure 3 presents that such distributions also depend on the size of particles due to the surface effects. For particles with the size of 4 nm and 5 nm the distributions are close with each other and close with those for the bulk [67]. Moreover, the distribution for Ti-O-Ti angle has two distinct peaks corresponding two common types of linking between octahedra in the system (i.e. via the edge and vertex) like those discussed above. Basing on the results

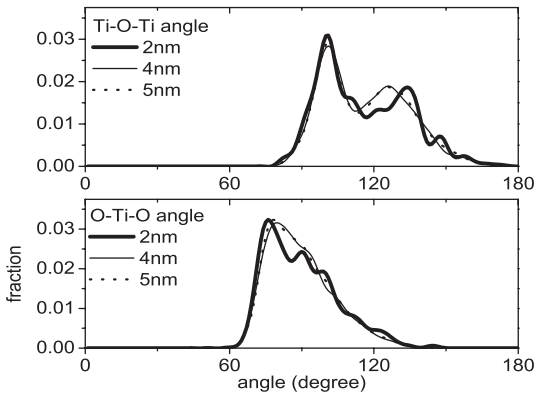

Fig. 3. Bond-angle distributions of amorphous TiO_2 nanoparticles at $T = 350$ K.

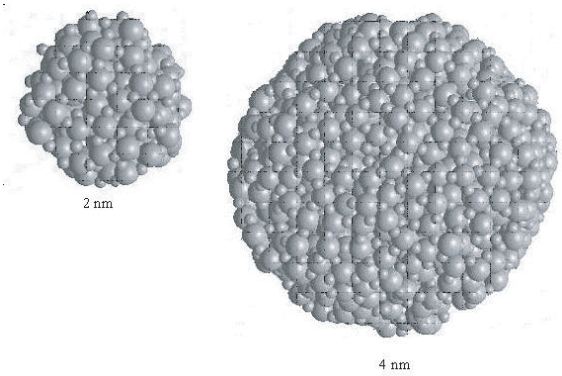

Fig. 4. Snapshot of amorphous TiO_2 nanoparticles at $T = 350$ K with the size of 2 nm and 4 nm, small spheres denote O atoms and the larger ones denote Ti atoms.

obtained above one can infer that although microstructure of amorphous TiO_2 nanoparticles changes significantly with the size due to the surface effects, their structure remains an octahedral network if the size is larger than 3 nm like those observed in the bulk. However, if the size is less than 2 nm structure of nanoparticles greatly differs from the bulk and it is close to the pentahedral network structure with the mean coordination number for the Ti-O pair equal to 5.30 (see Tabs. 2, 3). Snapshot for models with the size of 2 nm and 4 nm has been presented in Figure 4. One can see that at the surface atoms have more defects and hence it can be expected that the size of their cage is larger than that in the core of nanoparticles. And therefore, it can affect the diffusion of atoms in the surface area like that found for amorphous SiO_2 clusters [69]. Moreover, it seems that the surface of nanoparticles becomes much smoother if their size is larger (see Fig. 4). More details about the structure of an amorphous nanoparticle can be found via the study of structure in the surface area and in the core of particles (see below).

An important structural quantity of nanoparticle is the dependence of particle density $\rho(R)$ on the distance R from the center of nanoparticle. This quantity is determined as follows: we find the number of atoms belonging to the spherical shell with the thickness of 0.20 Å formed by two spheres with the radii of $R-0.10$ Å and $R+0.10$ Å.

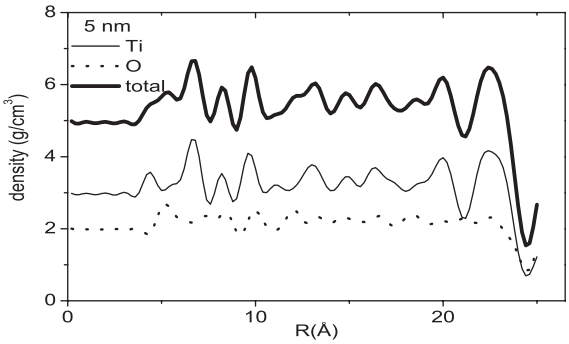

Fig. 5. Density profile in amorphous TiO_2 nanoparticles at the same $T = 350$ K.

Then we calculate the quantity $\rho(R)$. Here, it is unphysical if we begin for R from zero or from very small value since the number of atoms in any volume element is small, the local density is a rather noisy variable. The shells at the outer radii contain many more atoms than those near the center of nanoparticle and it is fair to carry out the accurate calculation of the outer part of the density profile for the largest nanoparticle with the size of 5 nm. Like those done in [83], we calculate directly $\rho(R)$ for the radii just beyond finite large enough value, which is taken equal to 4.00 Å in present work. The density profile has been averaged over three different configurations. Different configurations for model at 350 K have been obtained by different relaxation times. Inside 4.00 Å we take the smooth continuation of the density profile by the value of density, which is equal to the average density of spherical volume with the radius of 4.00 Å. This is essential to notice that the value 4.00 Å is equal to the cutoff radius for the calculating coordination number distribution for the Ti-Ti pair. The value of R increases from 4.00 Å with the step of 0.20 Å. As shown in Figure 5, $\rho(R)$ fluctuates around the value of 5.00 g/cm^3, which is higher than the density of an amorphous TiO_2 obtained in practice (i.e. it ranges from to 3.00 g/cm^3 to about 4.00 g/cm^3 depending on the fabricating method of samples [79]). Strong fluctuations of $\rho(R)$ indicate that our statistics are not good, smoother changes of the curves can be obtain via averaging over many independent runs. Oxygen atoms have a tendency to concentrate at the surface of nanoparticles like those observed at liquid SiO_2 or amorphous Al_2O_3 surfaces [69,71]. It can be seen clearly if one looks at the partial density profile for oxygen separately. The reason is that the system is energetically favored with an oxygen atom at the surface, since only one bond has to be broken if any, whereas if a titanium is at the surface several bonds have to be broken [69]. Due to the excess of oxygen at the surface, Ti atoms have a tendency to concentrate in the shell close to the surface in order to achieve the local charge neutrality [69,71]. And it causes a peak of the total density in the vicinity of the surface. Similar phenomenon has been found in liquid SiO_2 or amorphous Al_2O_3 surfaces [69,71]. However, unlike those observed in these works the density profile curves in our amorphous TiO_2 nanoparticles do not decrease down to zero at the surface (Fig. 5). This may

be related to the different boundary conditions used in simulations. In the present work, we do not use the periodic boundary conditions, however, during the relaxation process if atoms move out from the boundary of spherical nanoparticles those atoms have to be located right at the surface. Hence, significant amount of atoms in our nanoparticles is located right at the surface (Fig. 5). Overall, our results for the radial density profile in nanoparticle share many trends previously observed for free liquid non-spherical SiO_2 clusters [69] or amorphous Al_2O_3 thin film [71].

3.2 Surface structure of amorphous TiO_2 nanoparticles

Determination of the relationship between atomic surface structure and other physico-chemical properties of materials is one of the most important achievements of surface science. And due to mixing of ionic and covalent bonds in metal oxides such as TiO_2, surface structure has a strong influence on local surface chemistry compared to pure metals or elemental semiconductors [84]. Therefore, there is a large amount of works related to the study of surface of crystalline TiO_2 over the years (good review about surface science of crystalline TiO_2 of Diebold is strongly recommended [85]). However, there is no work related to the surface structure of an amorphous TiO_2. And hence, it is interesting to compare surface and core structures of nanoparticles with those for the bulk. To do it, we need a criterion to decide which atoms belong to the surface and which ones belong to the core of nanoparticles. There is no common principle for such choice of surface or core of the amorphous substances. Definition of thickness of the surface in [69] is somewhat arbitrary: all atoms that were within 5 Å of the hull just touched the exterior of droplet were defined belong to the surface, atoms that had the distance between 5 Å and 8 Å from the hull belong to the transition zone and remaining atoms belong to the interior. In contrast, no definition of surface has been clearly presented for the amorphous Al_2O_3 thin film; they used the top 1 Å or 3 Å layer of the amorphous thin film for surface structural studies [71]. From structure point of view it can be considered that atoms belong to the surface if they could not have full coordination and in contrast, atoms belong to the core if they can have full coordination for all atomic pairs like those in the bulk (i.e. the model with the periodic boundary conditions). And therefore, in present work atoms located in the outer shell of spherical nanoparticle with thickness of 4.00 Å (i.e. the largest radius of the coordination spheres used in the system) belong to the surface of nanoparticles and remaining atoms belong to the core.

As shown in Figure 6a and Table 4, the surface structure strongly depends on the size of nanoparticles and it differs from those for the bulk. However, if the size of nanoparticles larger than 4 nm the data are close with each other. Several remarks can be made here: the main peak in coordination number distributions for different atomic pairs in the surface shell shifts toward smaller value compared with those for the bulk indicating large amount of structural defects in the former due to breaking of bonds at the surface (i.e. undercoordinated units such as TiO_3 and TiO_4) with an exception for the O-Ti pair. However, increase number of O atoms with $Z_{O-Ti} = 1$ indicates the forming of dangling bonds at the surface like those observed at SiO_2 surface [69]. More details about the size dependence of surface structure can be found via the coordination number distribution for the Ti-O pair (Tab. 5).

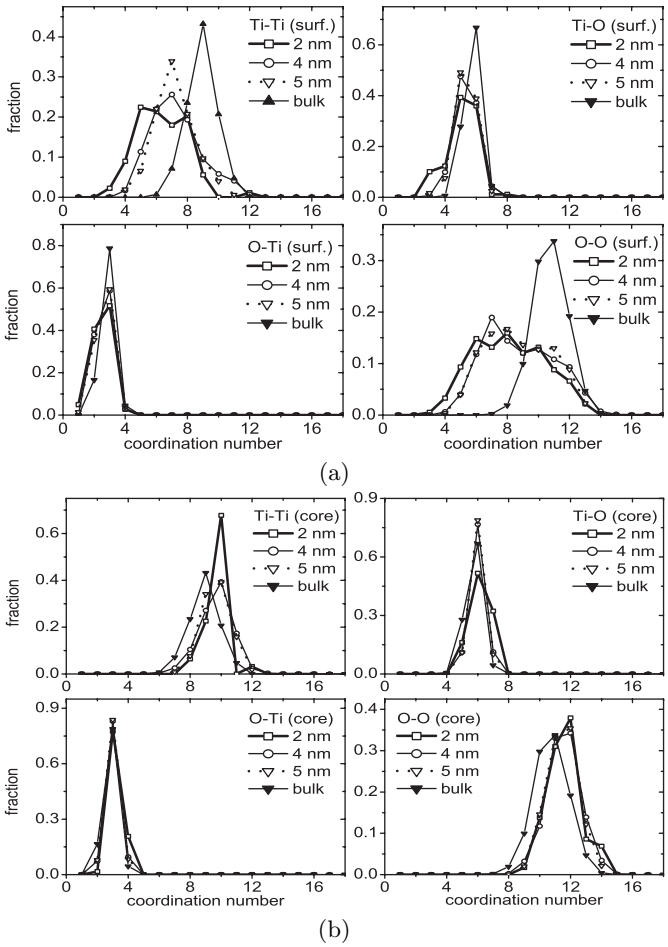

Fig. 6. (a) Coordination number distributions in the surface shell of amorphous TiO_2 nanoparticles compared with those in the amorphous bulk at $T = 350$ K [67]. (b) Coordination number distributions in the core of amorphous TiO_2 nanoparticles compared with those in the amorphous bulk at $T = 350$ K [67].

Table 4. Mean coordination numbers in the surface shell and in the core of nanoparticles at $T = 350$ K.

Materials		Z_{Ti-Ti}	Z_{Ti-O}	Z_{O-Ti}	Z_{O-O}
2 nm	Surface	6.44	5.06	2.51	8.15
	Core	9.57	6.08	3.11	11.51
3 nm	Surface	6.84	5.15	2.58	8.57
	Core	9.64	6.01	3.02	11.35
4 nm	Surface	7.17	5.30	2.64	8.77
	Core	9.67	6.00	3.02	11.49
5 nm	Surface	7.13	5.33	2.65	8.72
	Core	9.67	5.99	3.00	11.48

Table 5. Coordination number distribution for the Ti-O pair in the surface shell and in the core of nanoparticles at $T = 350$ K. We show the percentage of Ti atoms with corresponding value of Z_{Ti-O} which ranges from 3 to 8.

Materials		Z_{Ti-O}					
		3	4	5	6	7	8
2 nm	Surface	10.11	12.36	39.32	35.96	1.12	1.12
	Core	0.00	0.00	16.13	51.61	32.26	0.00
3 nm	Surface	1.74	16.52	47.82	31.30	2.61	0.00
	Core	0.00	0.00	4.57	84.57	10.86	0.00
4 nm	Surface	0.72	9.90	45.58	37.20	4.35	0.24
	Core	0.00	0.37	11.17	76.74	11.35	0.37
5 nm	Surface	1.70	7.56	49.23	38.89	2.47	0.15
	Core	0.00	0.00	11.00	78.81	10.02	0.16

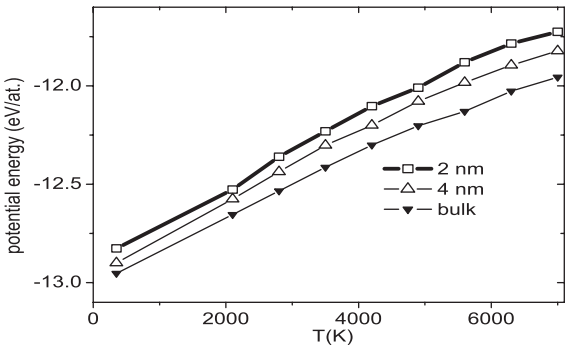

Fig. 7. Temperature dependence of potential energy per atom for the nanoparticle with two different sizes and for the bulk one [67]. The data have been accounted just for unrelaxed models.

One can see that structural units TiO_5 have their main fraction in the surface shell and coordination number distribution is broad due to the existence of undercoordinated structural units such as TiO_3, TiO_4. The existence of such structural defects in the surface shell of amorphous TiO_2 nanoparticles may enhance diffusion of atomic species compared with those in the core like those observed in silica nanoclusters [68,69]. Table 5 presents that if the size of nanoparticles is larger than 3 nm the coordination number distributions for Ti-O pair in the surface shell are similar with each other.

On the other hand, in an ideal octahedral network structure of crystalline TiO_2, titanium atoms are sixfold coordinated by oxygen and O atoms are threefold coordinated by titanium [85]. However, in an amorphous TiO_2 we found large amount of under- or overcoordinated structural units and percentage of Ti atoms with $Z_{Ti-O} = 6$ at 350 K is at around 67% [67]. And in amorphous TiO_2 nanoparticles such percentage is significantly lower compared with those observed in the bulk due to surface effects (see above). Therefore, Ti sites with $Z_{Ti-O} \neq 6$ and O sites with $Z_{O-Ti} \neq 3$ can be considered as structural point defects in amorphous TiO_2 nanoparticles (see Tabs. 3, 5), since under-coordinated Ti sites such as TiO_3, TiO_4 and TiO_5 can be can assumed as defects with oxygen deficiency like those discussed for crystalline TiO_2 [85]. In addition, due to lack of periodic order structure there is a possible large amount of another type of point defects in amorphous TiO_2 nanoparticles, i.e. vacancy like defects. One can find the existence of large pores at the surface of amorphous TiO_2 nanoparticles (see Fig. 4), such large pores can change their position with neighboring atoms and act as vacancy in diffusion process like those found and discussed previously for amorphous Al_2O_3 [75]. It seems that due to small dimension and specific amorphous structure there is an existence of only such typical point structural defects in the surface shells of amorphous TiO_2 nanoparticles unlike different types of structural defects observed in crystalline TiO_2 surfaces, i.e. step edges, oxygen vacancies, line defects, crystallographic shear planes etc. [85]. However, our understanding of structural defects in amorphous materials including those in amorphous surfaces is limited up to now and it needs a further study in this direction [75]. Further, one can find a large amount of structural defects in the surface shells of amorphous TiO_2 nanoparticles (Fig. 4 and Tab. 5) and they can have a strong influence on different properties of materials. For crystalline TiO_2, it was pointed out that defects can play a major role in a variety of surface phenomena [86], i.e. in bulk-assisted reoxidation [87,88], in restructuring and reconstruction processes [89,90] or in adsorption of sulfur and other inorganic compounds [91]. Similar phenomena for an amorphous TiO_2, probably, can be expected. On the other hand, imperfections of the surface structure of amorphous TiO_2 nanoparticles might lead to the changes in electronic structure of a sample like those observed for crystalline TiO_2 [85]. Moreover, while concentration of point defects in crystalline TiO_2 is typically reported as several percents [92,93], we found much larger amount of point defects in amorphous TiO_2 nanoparticles due to the surface structure contribution and their concentration strongly increases with decreasing nanoparticles size (see Tab. 5).

Figure 6b and Table 5 show that core structure of nanoparticles is also size dependent and close to that for the bulk, however, it differs significantly from the surface structure. Similar trends have been observed in crystalline nanoparticles [94]. The mean coordination number for Ti-O pair in the core of nanoparticles, Z_{Ti-O}, is equal to 6.00 versus about 5.76 in the bulk. Moreover, mean coordination number for other atomic pairs in the core is also higher than those in the bulk indicated the higher degree of an octahedrality of the nanoparticle core structure. One can see in Table 5 that fraction of octahedra TiO_6 dominates in the core of nanoparticles and it is nearly independent with particle size if it is larger than 3 nm.

And now, we would like to show the thermodynamics quantities of amorphous TiO_2 nanoparticles. The first quantity we would like to discuss here is the potential energy per atom, E_{pot}. We show temperature dependence of E_{pot} for nanoparticles with two different sizes together with ones for the bulk in Figure 7. One can see that E_{pot} for nanoparticles is significantly higher than that for the bulk due to the surface energy of the formers. Thus we

Table 6. Size dependence of thermodynamics quantities of nanoparticle at $T = 350$ K. Here, S/V is a ratio of surface area to volume of nanoparticle; E_T is the total energy per atom; E_s is the surface energy per unit area.

Size	S/V (Å^{-1})	E_T (eV/at.)	E_s (J/m^2)
2 nm	0.300	−12.781	0.582
3 nm	0.200	−12.825	0.571
4 nm	0.150	−12.851	0.523
Bulk [67]		−12.908	

can suggest the relation:

$$E_{pot}^{nano} - E_{pot}^{bulk} = E_s/N \quad (2)$$

here, E_s is the surface energy of nanoparticle. In present work, we have calculated the value for E_s only for the models obtained at 350 K after relaxation of 50 000 MD steps. As shown in Table 6, E_s slightly changes with increasing nanoparticle size it is equal to the value of around 0.50 J/m^2. The value is very close to those obtained by calculations for the low index surfaces of anatase, i.e. it is equal to 0.35–0.81 J/m^2, or those for rutile, i.e. it is equal to 0.47–0.95 J/m^2, see more details in [29]. Moreover, the value for E_s obtained in present work at 350 K is also close to the experimental data for low indexed surfaces of anatase or rutile, i.e. it ranges from 0.44 to 1.09 J/m^2 for anatase [95] or from 0.31 to 1.65 J/m^2 for rutile [96]. Although there is no experimental data for surface energy of amorphous TiO_2 nanoparticle to compare, one can consider that the calculated E_s has a reasonable value, which is close to those for crystalline ones. This means that MA interatomic potentials are suitable for representing both the bulk and surface properties of amorphous TiO_2. Furthermore, total energy per atom of nanoparticle (E_T) also higher than that for the bulk due to the surface energy contribution and it decreases with increasing their size toward the value for the bulk (Tab. 6).

Finally, our calculations show that structure of amorphous TiO_2 nanoparticles is strongly size dependent due to surface structure contributions and it might lead to a finite-size dependence of different physico-chemical properties of samples. Perhaps, finite-size effects on the Raman spectrum of nanocrystalline anatase TiO_2 have been found [34]. Moreover, metastability of anatase TiO_2 nanoparticles as a function of pressure is also demonstrated to be size dependent, with smaller crystallites preserving the structure to higher pressures [34]. On the other hand, it was found that ultrasmall clusters have a different crystalline structure (anatase or rutile) depending on their dimensions [97]. This means that one can produce films with controlled nanostructure by selecting the clusters prior to deposition like those discussed in [97].

4 Conclusions

(i) Our calculations show that Matsui-Akaogi interatomic potentials describe well both the bulk and surface structure of amorphous TiO_2. It was found that the mean coordination number for all atomic pairs increase with increasing size of nanoparticles toward the value observed for the bulk due to reduction of surface effects. The phenomenon that octahedra TiO_6 linking via the edge or via common vertex has been found in amorphous TiO_2 nanoparticles like those observed in the bulk.

(ii) We found that the main structural units in the surface shell of nanoparticles are TiO_5, but in the core the TiO_6 units dominate. Coordination number distributions in the core of nanoparticles are close to those for the bulk. Size effects are significant for the surface structure, however, they are less pronounced for the core.

(iii) We found clearly size dependence of structure of amorphous TiO_2 nanoparticles due to surface structure contributions rather than due to surface energy and it might lead to finite size effects on various physical properties, stability, phase transition etc. of this important material like those observed in practice for nanocrystalline TiO_2 [17,34,39,40,45,47]. This means that our finding supports the conclusion in [97] that the role played by the surface energy in determining the cluster structure needs a very careful reconsideration [11].

(iv) Although amorphous TiO_2 nanoparticles have been obtained in practice, our understanding of structure of such important polymorph of TiO_2 nanoparticles is limited. Therefore, the knowledge about the atomic-scale investigations like those observed in present work could be quite valuable for synthesis-oriented researchers.

This work was done in the Computational Physics Lab of the College of Natural Sciences — National University of Hochi-Minh City (Vietnam).

References

1. W.F. Zhang, M.S. Zhang, Z. Yin, Q. Chen, Appl. Phys. B: Lasers Opt. **70**, 261 (2000)
2. T. Paunesku, T. Rajh, G. Wiederrecht, J. Maser, S. Vogt, N. Stojicevie, M. Protie, B. Lai, J. Oryhon, M. Thurnauer, G. Woloschak, Nature Mater. **2**, 343 (2003)
3. P.V. Kamat, N.M. Dimitrijevic, J. Solar Energy **44**, 83 (1990)
4. A.L. Linsebigler, G.Q. Lu, J.T. Yates, Chem. Rev. **95**, 735 (1995)
5. R.J. Gonzalez, R. Zallen, in *Amorphous insulators and semiconductors*, edited by M.F. Thorpe, M.I. Mitkova (Kluwer Academic, Netherlands, 1997), p. 395
6. M. Gratzel, Nature **414**, 338 (2001)
7. X.Z. Ding, X.H. Liu, J. Alloys Comp. **248**, 143 (1997)
8. J. Yang, S. Mei, J.M.F. Ferreira, J. Mater. Res. **17**, 2197 (2000)
9. J. Yang, S. Mei, J.M.F. Ferreira, J. Am. Ceram. Soc. **84**, 1696 (2001)
10. S.T. Martin, A.T. Lee, M.R. Hoffmann, Environ. Sci. Technol. **29**, 2567 (1995)

11. H. Zhang, J.F. Banfield, J. Mater. Chem. **8**, 20173 (1998)
12. B. Ohtani, Y. Okugawa, S. Nishimoto, J. Phys. Chem. **91**, 3550 (1987)
13. M.R. Ranade, A. Navrotsky, H.Z. Zhang, J.F. Banfield, S.H. Elder, A. Zaban, P.H. Borse, S.K. Kulkarni, G.S. Doran, H.J. Whitfield, PNAS 99, Suppl. **2**, 6476 (2002)
14. H. Zhang, J.F. Banfield, J. Chem. Mater. **14**, 4145 (2002)
15. P.E. de Jongh, D. Vanmaekelbergh, Phys. Rev. Lett. **77**, 3427 (1996)
16. P.D. Moran, J.R. Bartlett, J.L. Woolfrey, G.A. Bowmaker, R.P. Cooney, J. Sol-Gel Sci. Tech. **8**, 65 (1997)
17. R.J. Gonzalez, Ph.D thesis, Virginia Polytechnic Inst. State Univ., USA, 1998
18. T. Zeng, Y. Qiu, L. Chen, X. Song, Mater. Chem. Phys. **56**, 163 (1998)
19. B. Xia, H. Huang, Y. Xie, J. Mater. Sci. Eng. B **57**, 150 (1999)
20. L. Gao, Q. Zhang, J. Scripta Mater. **44**, 1195 (2001)
21. A.J. Maira, J.M. Coronado, V. Augugliaro, K.L. Yeung, J.C. Conesa, J. Soria, J. Catalysis **202**, 413 (2001)
22. Y. Zhang, A. Weidenkaff, A. Reller, Mater. Lett. **54**, 375 (2002)
23. M. Hirasawa, T. Seto, T. Orii, N. Aya, H. Shimura, Appl. Surf. Sci. **197–198**, 661 (2002)
24. B. Su, X. Liu, X. Peng, T. Xiao, Z. Su, Mater. Sci. Eng. A 349, **59** (2003)
25. Y. Gao, Y. Masuda, W.-S. Seo, H. Ohta, K. Koumoto, Ceram. Inter. **30**, 1365 (2004)
26. A. Pottier, S. Cassaignon, C. Chaneac, F. Villain, E. Tronc, J.-P. Jolivet, J. Mater. Chem. **13**, 877 (2003)
27. A.V. Bandura, J.D. Kubicki, J. Phys. Chem. B **107**, 11072 (2003)
28. C. Liang, Y. Shimizu, T. Sasaki, N. Koshizaki, J. Mater. Res. **19**, 1551 (2004)
29. A.S. Barnard, P. Zapol, Phys. Rev. B **70**, 235403 (2004)
30. K.T. Lim, H.S. Hwang, W. Ryoo, K.P. Johnston, Langmuir **20**, 2466 (2004)
31. J. Tang, F. Redl, Y. Zhu, T. Siegrist, L.E. Brus, M.L. Steigerwald, Nano. Lett. **5**, 543 (2005)
32. T.V. Ashworth, C.A. Muryn, G. Thornton, Nanotechnology **16**, 3041 (2005)
33. A.P. Popov, A.V. Priezzhev, J. Lademann, R. Myllyla, J. Phys. D: Appl. Phys. **38**, 2564 (2005)
34. V. Swamy, A. Kuznetsov, L.S. Dubrovinsky, R.A. Caruso, D.G. Shchukin, B.C. Muddle, Phys. Rev. B **71**, 184302 (2005)
35. V.N. Koparde, P.T. Cummings, J. Phys. Chem. B **109**, 24280 (2005)
36. Z. Liu, L. Hong, B. Guo, Power Sources **143**, 231 (2005)
37. K.D. Kim, S.H. Kim, H.T. Kim, Coll. Surf. A: Physicochem. Eng. Asp. **254**, 99 (2005)
38. H. Shin, H.S. Jung, K.S. Hong, J.-K. Lee, Sol. Stat. Chem. **178**, 15 (2005)
39. D. Nicolas, B. Masenelli, P. Melinon, E. Bernstein, C. Dujardin, G. Ledoux, C. Esnouf, J. Chem. Phys. **125**, 171104 (2006)
40. S.M. Woodley, S. Hamad, J.A. Mejias, C.R.A. Catlow, J. Mater. Chem. **16**, 1927 (2006)
41. M.-H. Liao, C.-H. Hsu, D.-H. Chen, Sol. Stat. Chem. **179**, 2020 (2006)
42. L. Zhao, J. Yu, Colloid, Interf. Sci. **304**, 84 (2006)
43. B. Jiang, H. Yin, T. Jiang, Y. Jiang, H. Feng, K. Chen, W. Zhou, Y. Wada, Mater. Chem. Phys. **98**, 231 (2006)
44. P. Hald, J. Becker, M. Bremholm, J.S. Pedersen, J. Chevallier, S.B. Iversen, B.B. Iversen, Sol. Stat. Chem. **179**, 2674 (2006)
45. V. Swamy, A. Kuznetsov, L.S. Dubrovinsky, P.F. McMillan, V.B. Prakapenka, G. Shen, B.C. Muddle, Phys. Rev. Lett. **96**, 135702 (2006)
46. Hari-Bala, Y. Guo, X. Zhao, J. Zhao, W. Fu, X. Ding, Y. Jiang, K. Yu, X. Ly, Z. Wang, Mater. Lett. **60**, 494 (2006)
47. A.S. Barnard, S. Erdin, Y. Lin, P. Zapol, J.W. Halley, Phys. Rev. B **73**, 205405 (2006)
48. E. Alonso, I. Montequi, S. Lucas, M.J. Cocero, J. Supercr. Fluids **39**, 453 (2007)
49. G. Madras, B.J. McCoy, `http://eprints.iisc.ernet.in/archive/00009450/01/amorphousTiO2-cgd-revised.pdf`
50. L.C. Chen, T. Rajh, W. Jager, J.M. Nedeljkovic, M.C. Thurnauer, Synchrotron Radiat. **6**, 455 (1999)
51. T. Rajh, J.M. Nedeljkovic, L.C. Chen, O. Poluektov, M.C. Thurnauer, J. Phys. Chem. B **103**, 3515 (1999)
52. K.D. Jang, S.-K. Kim, S.-J. Kim, J. Nanopart. Res. **3**, 141 (2001)
53. O. Palchik, I. Felner, G. Kataby, T. Prozorov, A. Gedanken, J. Mater. Res. **15**, 2176 (2000)
54. K.V.P.M. Shafi, A. Gedanken, R.B. Goldfarb, I. Felner, J. Appl. Phys. **81**, 6901 (1997)
55. A. Galashev, V. Polukhin, I. Izmodenov, O. Rakhmanova, Glass Phys. Chem. **32**, 99 (2006)
56. M. Matsui, M. Akaogi, Mol. Simul. **6**, 239 (1991)
57. D.W. Kim, N. Enomoto, Z. Nakagawa, K. Kawamura, J. Am. Ceram. Soc. **79**, 1095 (1996)
58. C.R.A. Catlow, C.M. Freeman, R.L. Royal, Physica B **131**, 1 (1985)
59. C.R.A. Catlow, R. James, Proc. R. Soc. Lond. A **384**, 157 (1982)
60. H. Sawatari, E. Iguchi, R.J.D. Tilley, Phys. Chem. Sol. **43**, 1147 (1982)
61. M. Mostoller, J.C. Wang, Phys. Rev. B **32**, 6773 (1985)
62. J.E. Post, C.W. Burnham, Am. Mineral. **71**, 142 (1986)
63. H.I. Roux, L.J. Glasser, J. Mater. Chem. **7**, 843 (1997)
64. V. Swamy, J.D. Gale, Phys. Rev. B **62**, 5406 (2000)
65. P.M. Oliver, G.W. Watson, E.T. Kelsey, S.C. Parker, J. Mater. Chem. **7**, 563 (1997)
66. D.R. Collins, W. Smith, *Council for the Central Laboratory of Research Councils*, Daresbury Research Report DL-TR-96-001, 1996
67. V.V. Hoang, Phys. Stat. Sol. B **244**, 1280 (2007)
68. D.A. Litton, S.H. Garofalini, J. Non-Cryst. Sol. **217**, 250 (1997)
69. A. Roder, W. Kob, K. Binder, J. Chem. Phys. **114**, 7602 (2001)
70. I.V. Schweigert, K.E.J. Lehtinen, M.J. Carrier, M.R. Zachariah, Phys. Rev. B **65**, 235410 (2002)
71. S.P. Adiga, P. Zapol, L.A. Curtiss, Phys. Rev. B **74**, 064204 (2006)
72. D.K. Belashchenko, Russ. Chem. Rev. **66**, 733 (1997)
73. K. Vollmayr, W. Kob, K. Binder, Phys. Rev. B **54**, 15808 (1996)
74. A. Kerrache, V. Teboul, D. Guichaoua, A. Monteil, J. Non-Cryst. Sol. **322**, 41 (2003)
75. V.V. Hoang, Phys. Rev. B **70**, 134204 (2004)
76. V.V. Hoang, D.K. Belashchenko, V.T. Mai Thuan, Physica B **384**, 249 (2004)

77. V.V. Hoang, N.N. Linh, N.H. Hung, Eur. Phys. J. Appl. Phys. **37**, 111 (2007)
78. A. Winkler, J. Horbach, W. Kob, K. Binder, J. Chem. Phys. **120**, 384 (2004)
79. D. Mergel, D. Buschendorf, S. Eggert, R. Grammes, B. Samset, Thin Solid Films **371**, 218 (2000)
80. V. Petkov, G. Holzhuter, U. Troge, Th. Gerber, B. Himmel, J. Non-Cryst. Sol. **231**, 17 (1998)
81. I. Manzini, G. Antonioli, D. Bersali, P. Lottici, G. Gnappi, A. Montenero, J. Non-Cryst. Sol. **192–193**, 519 (1995)
82. W.L. Bragg, *Atomic Structure of Minerals* (Cornell Univ. Press, NewYork, 1937)
83. J. Huang, L.S. Bartell, Mol. Structure **567–568**, 145 (2000)
84. M.A. Barteau, J. Vac. Sci. Technol. A **11**, 2162 (1993)
85. U. Diebold, Surf. Sci. Rep. **48**, 53 (2003)
86. U. Diebold, M. Li, O. Dulub, E.L.D. Hebenstreit, Surf. Rev. Lett. **5–6**, 613 (2000)
87. M.A. Henderson, Surf. Sci. **343**, L1156 (1995)
88. M.A. Henderson, Surf. Sci. **419**, 174 (1999)
89. M. Li, W. Hebenstreit, L. Gross, U. Diebold, M.A. Henderson, D.R. Jennison, P.A. Schultz, M.P. Sears, Surf. Sci. **437**, 173 (1999)
90. R.A. Bennett, P. Stone, N.J. Price, M. Bouker, Phys. Rev. Lett. **82**, 3831 (1999)
91. E.L.D. Hebenstreit, W. Hebenstreit, U. Diebold, Surf. Sci. **461**, 87 (2000)
92. J.M. Pan, B.L. Maschhoff, U. Diebold, T.E. Madey, J. Vac. Sci. Technol. A **10**, 2470 (1992)
93. M.A. Henderson, Surf. Sci. **355**, 151 (1996)
94. F. Delogu, Phys. Rev. B **72**, 205418 (2005)
95. M. Lazzeri, A. Vittadini, A. Selloni, Phys. Rev. B **63**, 155409 (2001); M. Lazzeri, A. Vittadini, A. Selloni, Phys. Rev. B **65**, 119901 (2002)
96. M. Ramamoorthy, D. Vanderbilt, R.D. King-Smith, Phys. Rev. B **49**, 16721 (1994)
97. E. Barborini, I.N. Kholmanov, P. Piseri, C. Ducati, C.E. Bottani, P. Milani, Appl. Phys. Lett. **81**, 3052 (2002)